Applied Catalysis B: Environmental 203 (2017) 65–71

Contents lists available at ScienceDirect

Applied Catalysis B: Environmental

journal homepage: www.elsevier.com/locate/apcatb

Incorporating a novel metal-free interlayer into g-C_3N_4 framework for efficiency enhanced photocatalytic H_2 evolution activity

Weinan Xing, Chunmei Li, Gang Chen*, Zhonghui Han, Yansong Zhou, Yidong Hu, Qingqiang Meng

MIIT Key Laboratory of Critical Materials Technology for New Energy Conversion and Storage, School of Chemistry and Chemical Engineering, Harbin Institute of Technology, 150001, PR China

ARTICLE INFO

Article history:
Received 2 August 2016
Received in revised form
27 September 2016
Accepted 30 September 2016
Available online 4 October 2016

Keywords:
g-C_3N_4 photocatalyst
Metal-free interlayer
Adjust band gap
Effective charge separation
Photocatalytic properties

ABSTRACT

Graphitic carbon nitride (g-C_3N_4) has become a research hotspot recently owing to its unique advantage and wide application in the field of photocatalysis. However, the photocatalytic activity of the traditional two-dimensional g-C_3N_4 material is unsatisfactory owing to the relatively narrow visible light responsive region and high recombination probability of photogenerated charge carriers. Here, the novel nonmetal interlayer incorporated into the g-C_3N_4 framework is successfully fabricated by thermal polymerization of the β-cyclodextrin (β-CD) and melamine as precursors, which significantly enhances the photocatalytic performance for H_2 evolution than that from g-C_3N_4. The corresponding characterization methods demonstrate that the interlayer is composed of oxygen-contained graphitized carbon as well as the enhanced photocatalytic activity originates from the narrowed band gap, negative-shifted conduction band position and efficient charge transfer caused by this metal-free interlayer incorporation. It not only results in the form of the C—O—C bonding between the interlayer and g-C_3N_4 but also can bridge the interlayer and extend the π-conjugated system, which facilitate the charge-carrier migration and separation. The current work could provide new insights for constructing other high performance, low-cost and metal-free photocatalyst for H_2 evolution.

1. Introduction

Hydrogen (H_2), as one of the most promising replacement energy, attracts enormous interests due to its environmental friendly and renewable. Photocatalytic H_2 evolution from the water by using the sunlight as the only source of energy has been treated as the major trend [1]. Therefore, the design and development of low-cost, highly-efficient and eco-friendly photocatalysts have become the most research hotspot in the photocatalytic fields [2]. Graphitic carbon nitride (g-C_3N_4) has aroused tremendous interest because of its well-suited band positions (about 2.7 eV) for effective absorption of sunlight since it was first reported as a significant photocatalyst in 2009 [3]. Especially, many extraordinary advantages inspired the enthusiasm of researchers: such as its low-priced raw material, simple preparation method, good thermal and chemical stability et al. [4,5] Given the favorable features, g-C_3N_4 is regarded as a promising candidate for the photocatalytic H_2 production from the water. However, the insufficient optical absorption in the visible region and the small specific surface area of pure g-C_3N_4 limit the practical application [6,7]. Meanwhile, the weak van der Waals interaction between neighbouring g-C_3N_4 layers restrict the electron coupling between the layers, which have negatively effect on the electron transfer and weaken the photocatalytic activity [8]. Therefore, the key solution instrumentals of these problems are relying on regulating the electronic structures to narrow the band gap, change the morphology to enlarge the specific surface area and promote the separation of electron-hole to enhance the photocatalytic activity.

As a typical layered material, the large interlayer space and the weak van der Waals force between the neighbouring layers of g-C_3N_4 are beneficial for the formation of intercalation material with promising properties. Very recently, Dong et al. have demonstrated the synthesis of K-intercalated g-C_3N_4 photocatalyst, which extended the π conjugated system of g-C_3N_4 and showed the improvement of photocatalytic activity for the removal of NO [9]. Zou et al. also prepared the alkali metal salts intercalated g-C_3N_4, which promoted the separation and transport of photogenerated carriers efficiently and thus improved the photocatalytic hydro-

* Corresponding author.
E-mail address: gchen@hit.edu.cn (G. Chen).

http://dx.doi.org/10.1016/j.apcatb.2016.09.075
0926-3373/

gen evolution [10]. All the above results obviously proved that the preparation of intercalated g-C_3N_4-based photocatayst is a smart and efficient way to raise the photocatalytic activity of g-C_3N_4. Nevertheless, in contrast with the current reported metal interlayer g-C_3N_4-based photocatayst, the metal-free interlayer into g-C_3N_4 framework is rarely reported. Compared with the metal-based materials, the metal-free material has the advantage in eco-friendly, economic and sustainable value. In addition, as the nonmetal interlayer, it may be easily to form the covalent bond with the adjacent C/N atoms in the framework, which facilitate the electron coupling between the layers. It would have the positive effect on the electron transfer and improve the photocatalytic activity. Therefore, the construction of metal-free interlayer g-C_3N_4 may have the significant effects on the improve its photocatalytic activity and extend its applied range for the practical requirement.

Carbonaceous materials, as their unique properties like chemical stability, good conductivity and low cost, have drawn much research attentions in recent years. It has been demonstrated that the introduction of carbon materials influences the performance of the photocatalyst [11]. β-cyclodextrin (β-CD) as a class of cyclic oligosaccharides consisting of several α(1 → 4)-linked glucopyranose units, has been widely used as carbon precursors to afford carbon dots [12], carbon nanowire [13] and carbon nanoporous materials [14], and so forth. In addition, β-CD is an oxygen-rich carbon precursor and has a relatively larger number of hydroxy groups in the structure, which is easily to obtain oxygen-doped carbon materials. On one hand, some studies have been reported that the presence of heteroatom species (N, O, S) and functional groups on carbon matrix participate in the charge-transfer reactions, which can improve the electrical conductivity of the materials[15–17]. On the other hand, the hydroxy groups of β-CD are easy to form H-bands with melamine (the precursor of g-C_3N_4) and participate in the polymerization reaction of g-C_3N_4-based materials. In addition, several researches have used the β-CD to prepare intercalated materials [18,19]. Inspired by these, we speculate that the using of β-CD and melamine as the precursor to prepared the metal-free intercalated g-C_3N_4 photocatalyst may have significant impact on improving the photocatalytic activity of g-C_3N_4.

In this work, for the first time, the metal-free interlayer which used the β-CD as the source is incorporated into the g-C_3N_4 interlamination through the thermal polymerization strategy. The Fourier transform infrared spectra, thermogravimetric analysis and X-ray photoelectron spectroscopy measurements have demonstrated that the metal-free interlayer is composed of oxygen-contained graphitized carbon. We have an insight into the influence of the incorporation of nonmetal interlayer on g-C_3N_4 morphology, structure, optical and electronic properties. Interestingly, it is found that this metal-free interlayer incorporation not only adjusted the energy band structure of g-C_3N_4 by simply changing the ratio of the original materials, but also bridge and extend the π-conjugated system of g-C_3N_4 network to promote the effective separation of charge-carrier. As expected, the as-prepared photocatalysts exhibit superior photocatalytic activity of H_2 evolution under the visible light. At last, the possible photocatalytic H_2 evolution mechanism is performed.

2. Experimental

2.1. Synthesis of photocatalysts

To synthesize the oxygen-contained graphitized carbon intercalated g-C_3N_4, melamine (5.00 g) and different weight ratios of β-cyclodextrin (β-CD) were dispersed in 30 mL deionized water with stirring at 80 °C water bath to completely remove the water. Then, the obtained solid mixture was put into an alumina crucible with a cover and calcined at 600 °C for 2 h with a ramping rate of 5.0 °C min^{-1}. The mass ratio of β-CD to melamine was changed from 0.5% to 2%, which the obtaining photocatalysts were denoted as g-C_3N_4-0.5, g-C_3N_4-1 and g-C_3N_4-2, accordingly. For comparison, the pure g-C_3N_4 was prepared by directly heating melamine under the same procedure.

2.2. Characterization

The X-ray diffraction (XRD) patterns were obtained on RigakuD/max-2000 X-ray diffractometer and equipped with a Cu-Kα radiation. Fourier transform infrared (FT-IR) spectra were studied with IR Affinity-1 spectrometer in the range of 500–4000 cm^{-1}, using KBr pellets. Transmission electron microscopy (TEM) was performed on the FEI Tecnai G2 S-Twin. X-ray photoelectron spectroscopy (XPS) analysis was recorded on an American electronics physical HI5700ESCA system with X-ray photoelectron spectroscope using Al K (1486.6 eV) monochromatic X-ray radiation. The N_2 adsorption-desorption isotherms were measured by an AUTOSORB-1-MP surface analyzer at 77 K. The UV–vis diffuse reflectance spectra (DRS) were tested on a UV–vis spectrophotometer (PG, UH-4150) at room temperature. Thermo gravimetric-differential scanning calorimetry analysis (TG-DSC) was measured on a SDT Q600 TG-DSC Instruments. The photoluminescence (PL) spectra were carried out on FLUOROMAX-4C-TCSPC at room temperature.

2.3. Photocatalytic test

The photocatalytic hydrogen evolution was tested using a gas-tight circulation system with a side window. The visible light irradiation was acquired by a 300 W Xenon lamp (Trusttech PLS-SXE 300, Beijing) light source with a cut off filter (λ > 400 nm). The light density is 87 mW/cm^2 in the photocatalytic test section. In each experiment, 0.1 g photocatalyst and 300 mL aqueous solution were introduced into the quartz glass reactor. Meanwhile,10 vol% of triethanol amine solution (TEOA solution) and $H_2PtCl_6{\cdot}6H_2O$ (Pt, 3 wt%) were also used as a sacrificial agent and co-catalyst. Prior to irradiation, the suspension was degassed with N_2 for several times to remove the O_2 completely inside the reactor. The amount of H_2 production was analyzed by gas chromatography (Agilent 7890) with a thermal conductivity detector (TCD), and Ar was used as the carrier gas.

2.4. Photoelectrochemical measurements

Photoelectrochemical measurements were carried out on CHI604C electrochemical workstation with a conventional three-electrode cell. In this electrochemical system, a Pt pole as the counter electrode (CE), Ag/AgCl electrode as the reference (RE), and the as-prepared sample electrode coated at FTO glass electrode as the working electrode (WE). 0.5 M Na_2SO_4 aqueous solution (50 mL) was used as the electrolyte. A 300 W Xe lamp (Trusttech PLS-SXE 300, Beijing) with cutoff filter (λ > 400 nm) were used as the visible light source. The working electrodes were prepared in a typical method: 20 mg photocatalyst was mixed with 300 μL terpilenol to obtain a slurry. Then the resulting slurry was dropped on FTO glass electrode by the spin coater and dried at 80 °C.

3. Results and discussion

3.1. Structure and morphology

The crystal structure of pure g-C_3N_4 and metal-free intercalated g-C_3N_4 are studied through XRD patterns, as shown in Fig. 1. The peaks at 12.8° (100) and 27.8° (002) are related to the in-plane

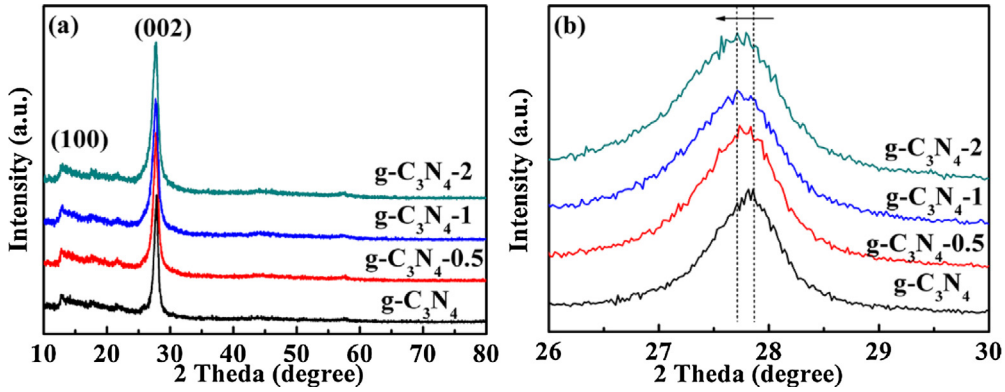

Fig. 1. XRD patterns (a) and magnified peaks at (002) (b) of g-C_3N_4, g-C_3N_4 −0.5, g-C_3N_4–1 and g-C_3N_4 −2.

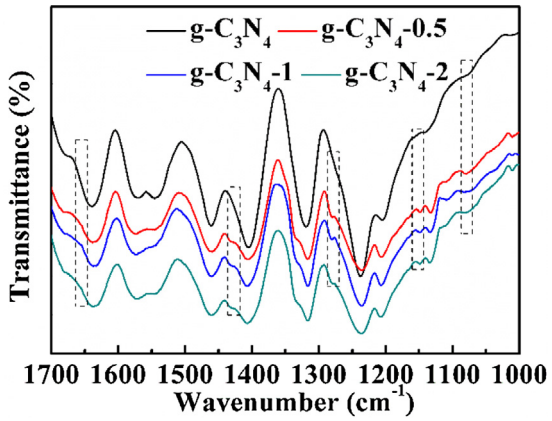

Fig. 2. Magnified FT-IR spectra of g-C_3N_4, g-C_3N_4 −0.5, g-C_3N_4–1 and g-C_3N_4 −2.

repeated units and the interlayer stacking reflection in g-C_3N_4 [20]. The similar diffraction peaks of (100) and (002) indicate that the original crystal structure of g-C_3N_4 is well-maintained after the incorporation of metal-free interlayer. With increasing metal-free intercalated amount, the magnified view of (002) diffraction peaks (Fig. 1b) show regularly shift toward lower angles compared with pure g-C_3N_4. According to Bragg's law, the decrease in 2 θ values indicates the increment of the interlayer distance [21]. This may be due to the metal-free interlayer has been incorporated into the g-C_3N_4 and bonded with the adjacent C or N atoms, which enlarged the interlayer distance. This phenomenon has been observed in other intercalated g-C_3N_4 [9,22]. These XRD results indicate that the metal-free interlayer may have been well incorporated into the g-C_3N_4, but its main chemical skeleton of g-C_3N_4 has been retained. In addition, the FT-IR spectra further confirm the presence of metal-free interlayer into g-C_3N_4. As shown in Fig.S1, the strong characteristic peaks in the 1200–1700 cm^{-1} region are related to typical C—N heterocyclic stretches of the triazine (C_6N_7) ring [23]. The peak at 807 cm^{-1} is derived from the breathing vibration of the heptazine units. The broad peak ranging from 3200 to 3400 cm^{-1} can be related to the N—H and O—H components. Notably, the photocatalysts show the similar characteristic peaks except several extra peaks appeared on metal-free intercalated g-C_3N_4 from the enlarged FT-IR spectra in Fig. 2. The peaks at 1655 cm^{-1} and 1435 cm^{-1} are related to the C=C skeletal vibration band of aromatic ring, while the peaks at 1280 cm^{-1}, 1150 cm^{-1} and 1075 cm^{-1} are related to C—O—C stretching, C—C band, and phenolic C—OH stretching [21,24], further supports the existence of metal-free interlayer in the g-C_3N_4 framework and the metal-free interlayer is composed of oxygen-contained graphitized carbon.

The microstructure of pure g-C_3N_4 and metal-free intercalated g-C_3N_4 are studied by TEM and SAED (insert) images. As shown in Fig. 3, the metal-free intercalated g-C_3N_4 sample exhibits the similar morphology with pure g-C_3N_4, indicating the introduction of metal-free interlayer don't destroy the microstructure of g-C_3N_4. The insets of SAED in Fig. 3a and b confirm the polycrystalline nature of g-C_3N_4 and metal-free intercalated g-C_3N_4. The metal-free interlayer of oxygen-contained graphitized carbon is incorporated into the g-C_3N_4 and bonded with the adjacent C or N atoms. Thus, a higher crystallinity of metal-free intercalated g-C_3N_4 is observed.

The XPS measurements are used to obtain more information about the chemical composition and surface states of pure g-C_3N_4 and metal-free intercalated g-C_3N_4 (Fig. 4). By employing a Gaussian curve fitting approach, the high resolution C 1 s spectra are fitted into three peaks centering at 284.8 eV, 286.2 eV and 288.4 eV for both photocatalysts as well as two new peaks at 287.9 eV and 289.5 eV for metal-free intercalated g-C_3N_4. The peak at 288.4 eV is assigned to sp^2-hybridized carbon in N containing aromatic ring, while the peak in 286.2 eV is attributed to the sp^2C atoms in the aromatic ring attached to the $-NH_2$ group. Moreover, The peak centered at 284.8 eV can be ascribed to surface adventitious carbon or sp^2 C—C bonds on oxygen-contained graphitized carbon [25]. For the metal-free intercalated g-C_3N_4, the new peaks in 289.5 eV and 287.9 eV are corresponding to the O—C=O and O=C bonds, which are consistent with the O1s spectrum in Fig. 3b. Obviously, the peak of O 1s in metal-free intercalated g-C_3N_4 is stronger than that of pure g-C_3N_4, suggesting that the higher oxygen content in metal-free intercalated g-C_3N_4. For pure g-C_3N_4, the O 1s cored at 532.3 eV is stem from the adsorbed water. Particularly, two new peaks at 531.8 eV and 532.9 eV are detected in metal-free intercalated g-C_3N_4, attributed to the O—C=O and C—O groups [26]. These results further indicated that the metal-free interlayer is composed of oxygen-contained graphitized carbon, which is consisted with the result of FT-IR analysis.

Specifically, the deconvolution of the N 1s spectrum is achieved four styles of N species, that is, the sp^2 bonded N in the triazine rings (398.9 eV), bridging N atoms in N-$(C)_3$ (400.5 eV), N atoms bonded with H atoms (401.6 eV) and the charging effects (404.5 eV) [5]. Notably, there are obvious chemical shifts of N 1s and C 1s in comparison with pure g-C_3N_4. Both of the observation shifts of N 1s and C 1s further testify the strong interaction between metal-free interlayer and the adjacent C/N atoms in the sample [9,27]. Based on the above analysis, we may conclude that the metal-free interlayer composed of oxygen-contained graphitized carbon is successfully incorporated into the g-C_3N_4 framework.

The thermal stability of pure g-C_3N_4 and metal-free intercalated g-C_3N_4 are demonstrated by thermogravimetric analysis (TGA). As shown in Fig. S2, both of the TGA curves show no obvious weight loss until 550 °C, which prove the better thermal stability

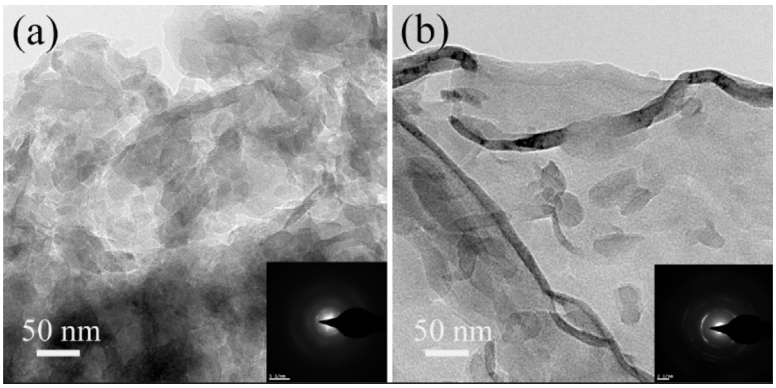

Fig. 3. TEM and SAED (insert) images of g-C_3N_4(a) and g-C_3N_4 −1(b).

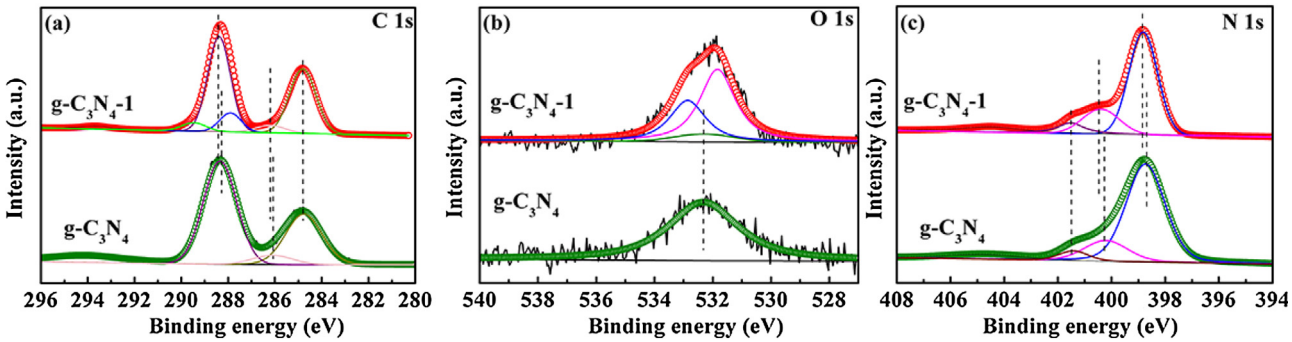

Fig. 4. High-resolution XPS spectra of C 1s (a), O 1s (b) and N 1 s (c) of g-C_3N_4 and g-C_3N_4 −1.

of the materials. However, when the temperature reaches 720 °C, a drastic weight loss is observed, which may be attributed to the decomposition of g-C_3N_4 [28]. For metal-free intercalated g-C_3N_4, a faster decomposition is observed at a relatively low temperature than pure g-C_3N_4, which is related to the incorporation of metal-free interlayer into g-C_3N_4. The reason can be classified into two parts, one is attributed to the existence oxygen functional groups in graphitized carbon, which may accelerate the metal-free intercalated g-C_3N_4 decomposition at a relatively low temperature [29]. The other is due to the presence of metal-free interlayer in the g-C_3N_4 and decrease the stability of g-C_3N_4, which lead to the decomposition of metal-free intercalated g-C_3N_4 at a relatively low temperature [9].

3.2. Optical Property

The UV–vis DRS spectra of pure g-C_3N_4 and metal-free intercalated g-C_3N_4 are measured to evaluate light absorption property. As shown in Fig. 5, the pure g-C_3N_4 shows the typical absorption edge at about 470 nm, which is well consistent with the reported value [30]. However, when the metal-free interlayer has been incorporated into g-C_3N_4, the significant red-shift to longer wavelength is observed. At the same time, the absorption intensities significantly improve in the visible light region, which are consistent with the colors change from yellow to dark green with the increasing of weight ratio of β-CD in the precursor (Fig. S3). As we all known, the red-shift of the wavelength always means the band gap narrowing of the photocatalysts. Therefore, the plots of $(\alpha h\nu)^2$ versus $h\nu$ are used to determined the band gaps value of the as-prepared photocatalysts. As shown in Fig. 5b. the values of band gaps are determined to be about 2.78 eV, 2.75 eV, 2.62 eV and 2.55 eV, which exhibit the band gaps narrowing with the increasing metal-free intercalated amount. The band gaps narrowing phenomenon results from the existence of oxygen-contained graphitized carbon. The oxygen-contained graphitized carbon plays a key role to form C—O—C covalent bonding with g-C_3N_4 interlayer during thermal conversion, which narrow the band gap and enhance the visible light absorption [31,32]. The above results suggest that the interaction of oxygen-contained graphitized carbon with g-C_3N_4 interlayer should be the formation of chemical bonding rather than $\pi - \pi$ simple stacking, which is consistent with the XPS and FT-IR results. Decreased band gap and enhanced light harvesting ability are both beneficial to enhancing the photocatalytic activity of g-C_3N_4.

Besides a suitable bandgap, the matching levels of conduction band (CB) and valence band (VB) are also important for the photocatalytic reaction. To verify the relative positions of CB and VB edges, Mott- Schottky plots and XPS valence band spectra are used. In general, the flat-band potential can be used to approximately estimate the CB position [33]. As shown in Fig. 6, the g-C_3N_4 and metal-free intercalated g-C_3N_4 exhibit the positive slope in the linear region, indicating they are n-type semiconductors. Based on these plots, the flat band potentials are estimated to be −0.97 V, −1.08 V, −1.17 V and −1.03 V for g-C_3N_4, g-C_3N_4-0.5, g-C_3N_4-1 and g-C_3N_4-2, respectively. Obviously, the potential of CB in the metal-free intercalated g-C_3N_4 occur to negative shift compared to pure g-C_3N_4. The more negative potential of CB could enhance the reduction capability of electrons, which is beneficial for the facilitating of the photocatalytic H_2 evolution. In addition, the XPS valence band spectra is used to further determine the VB level. Fig. S4 shows that the potential of VB occur to negative shift in the metal-free intercalated g-C_3N_4, which is consistent with the potential of CB results. Based on the above data, combined with the bandgap energy, the band structure of the as-prepared photocatalysts can also be obtained (Fig. 6e), both of the CB and VB potentials are altered after nonmetal oxygen-contained graphitized carbon incorporation. Hence, we may conclude that the incorporation of metal-free interlayer can significantly adjust the band structure of

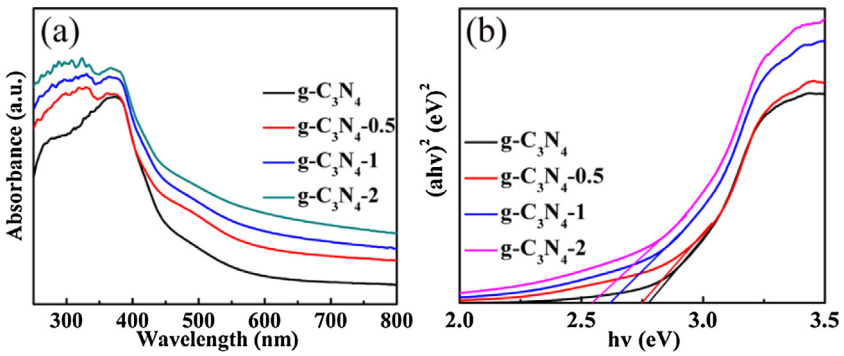

Fig. 5. UV–vis DRS (a) and $(\alpha h\nu)^2$ versus $h\nu$ (b) of g-C_3N_4, g-C_3N_4 −0.5, g-C_3N_4–1 and g-C_3N_4 −2.

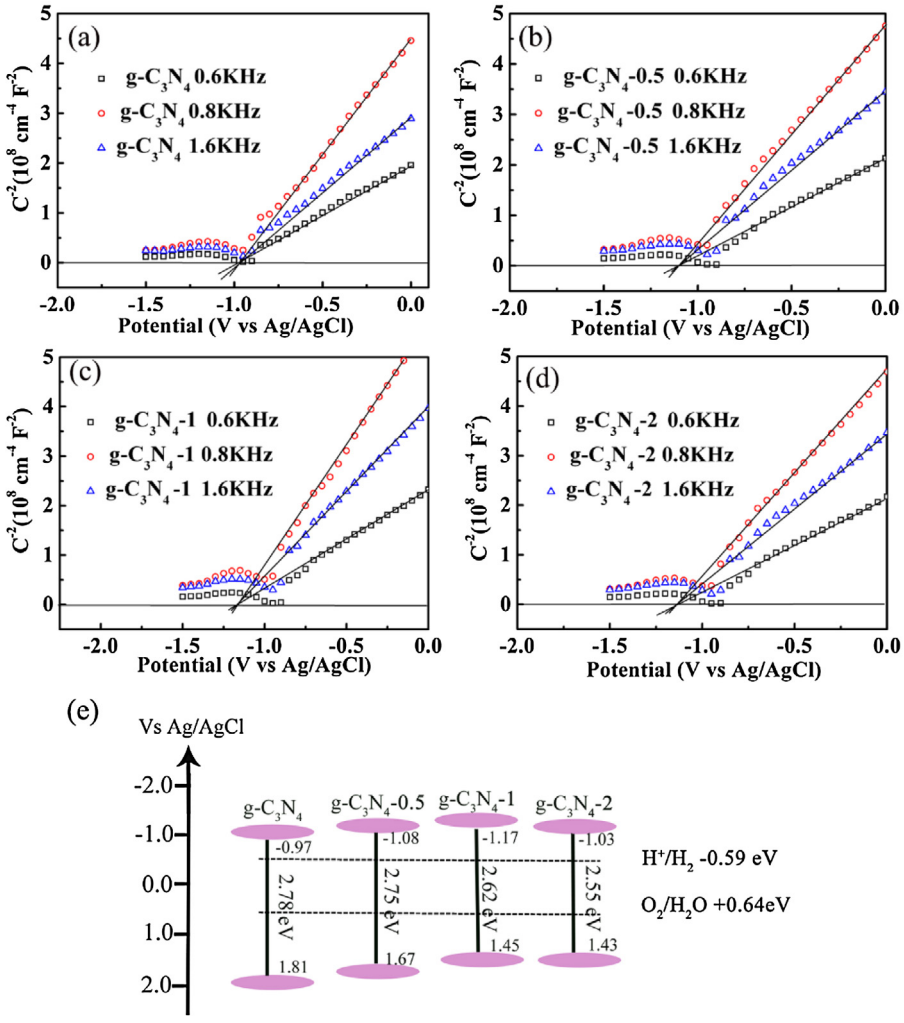

Fig. 6. Mott–Schottky plots (a-d) and schematic illustration of the band structure (e) of g-C_3N_4, g-C_3N_4 −0.5, g-C_3N_4–1 and g-C_3N_4 −2.

g-C_3N_4 and negative shift the potential of CB, which is important for the improvement of photocatalytic activity of H_2 evolution.

3.3. Photocatalytic Properties

The photocatalytic performances of the as-prepared photocatalysts have been tested by H_2 evolution under visible-light irradiation ($\lambda > 400$ nm). As can be observed from Fig. 7, all the metal-free intercalated g-C_3N_4 photocatalysts show the higher H_2 evolution activity compared with the pure g-C_3N_4. In particular, the g-C_3N_4-1 shows the highest H_2 evolution rate of 793 μmol h^{-1} g^{-1}, which is about 5 times higher than that of pure g-C_3N_4. The enhancement of photocatalytic H_2 evolution may be due to the introduction of metal-free interlayer into g-C_3N_4. On one hand, the incorporation of metal-free interlayer not only narrow the band gap and enhance the visible light harvesting, but also upshift of the CB potential to improve the reduction capability of electrons. On the other hand, metal-free interlayer incorporated into g-C_3N_4, which bridged the g-C_3N_4 interlayer and extended the π-conjugated system of g-C_3N_4, thus facilitate the separa-

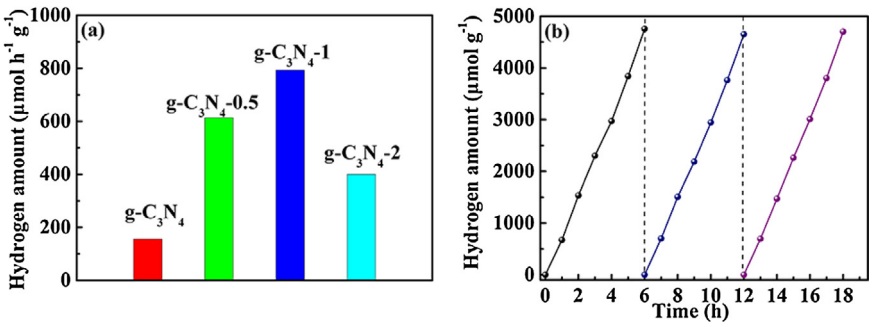

Fig. 7. Photocatalytic H_2 evolution rate of (a) g-C_3N_4, g-C_3N_4 −0.5, g-C_3N_4–1 and g-C_3N_4 −2. under visible light irradiation and (b) Recycle of H_2 evolution of g-C_3N_4 −1.

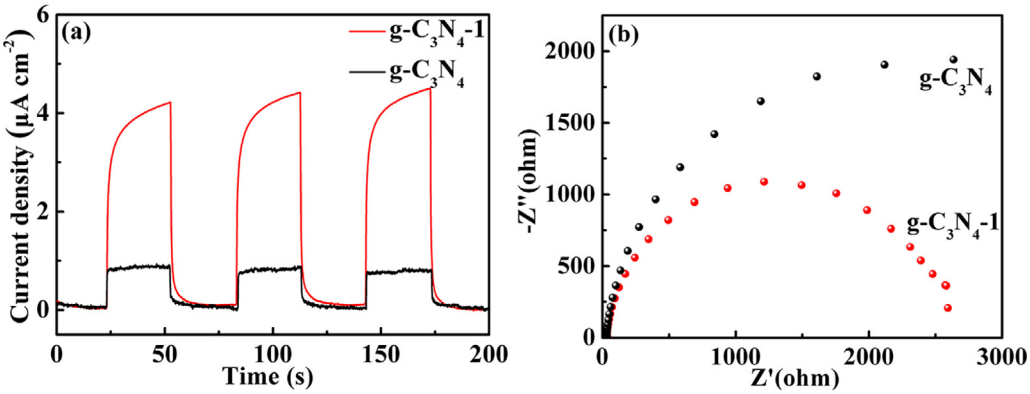

Fig. 8. Photocurrent responses (a) and EIS plots (b) of g-C_3N_4 and g-C_3N_4 −1.

tion efficiency of charge carriers. As an important parameter for the improvement of photocatalytic activity, the N_2 adsorption-desorption experiments are carried out (Fig.S5). After calculation, the BET surface areas of pure g-C_3N_4 and g-C_3N_4-1 are 18.12 $m^2\ g^{-1}$ and 34.89 $m^2\ g^{-1}$, respectively. Through normalized with the surface areas of the two photocatalysts, the hydrogen evolution rates are 8.62 $\mu mol\ h^{-1}\ g^{-1}\ m^{-2}$ and 22.73 $\mu mol\ h^{-1}\ g^{-1}\ m^{-2}$ for pure g-C_3N_4 and g-C_3N_4-1. It suggested that the BET surface area is another reason for the enhancement of photocatalytic H_2 evolution. In addition, the photocatalytic activity of the as-prepared photocatalysts are also evaluated under visible light (λ> 420 nm). As shown in Fig. S6, the reaction rate of metal-free interlayer g-C_3N_4 photocatalysts is 213.2 $\mu mol\ h^{-1}\ g^{-1}$, 258.5 $\mu mol\ h^{-1}\ g^{-1}$ and 163.0 $\mu mol\ h^{-1}\ g^{-1}$ for g-C_3N_4 −0.5, g-C_3N_4–1 and g-C_3N_4 −2, which are all higher than that of pure g-C_3N_4. At last, the durability of metal-free intercalated g-C_3N_4 is also tested by recycling the photocatalyst for the H_2 evolution. The amount of H_2 production increase stably with prolonged the irradiation time and without noticeable deactivation is observed after 3 cycles, which confirms that metal-free intercalated g-C_3N_4 is a stable photocatalyst during the photocatalytic H_2 evolution.

To better confirm and understand the enhanced excitation, separation and migration of the photo-induced charge carriers of g-C_3N_4 and metal-free intercalated g-C_3N_4, photoelectrochemical measurements are recorded. As shown in Fig. 8a, both of the two photocatalysts show rapid and consistent photocurrent responses for each light on and off under visible light. Notably, an enhanced photocurrent intensity for metal-free intercalated g-C_3N_4 electrode is observed, which is nearly 4 times higher than that of pure g-C_3N_4. It suggests the more efficient separation of electrons and holes in metal-free intercalated g-C_3N_4 [34]. Meanwhile, to gain deeper insights into the charge transport behavior of g-C_3N_4 and metal-free intercalated g-C_3N_4 in the absence of light excitation, the conducted electrochemical impedance spectroscopy (EIS) measurements were examined under dark conditions. Compared with pure g-C_3N_4, a smaller diameter of metal-free intercalated g-C_3N_4 is observed, suggesting that the incorporation of oxygen-contained graphitized carbon into g-C_3N_4 interlayer can effectively enhance the electronic conductivity of polymer matrix and accelerate the rate of charge transfer towards the photocatalytic H_2 evolution. In order to verify the conclusion, we compared the electrochemical hydrogen evolution activities of g-C_3N_4 and metal-free intercalated g-C_3N_4 using the linear sweep voltammetry (LSV) technique. As show in Fig. S7, the metal-free intercalated g-C_3N_4 demonstrated much improved electrochemical hydrogen evolution activity. Additionally, the photoluminescence (PL) spectra are used to further provide information on the migration, transfer and separation efficiency of photo-excitation electrons and holes in the photocatalyst because PL emission mainly arises from the charge carrier recombination [35]. As shown in Fig. 9, the pure g-C_3N_4 shows a main emission peak at approximately 470 nm, which is due to the direct electrons and holes recombination of band transition [36]. Com-

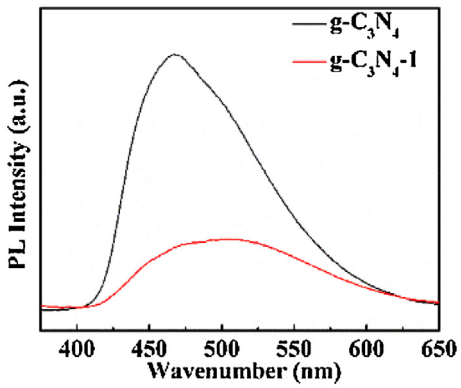

Fig. 9. PL spectra of g-C_3N_4 and g-C_3N_4 −1.

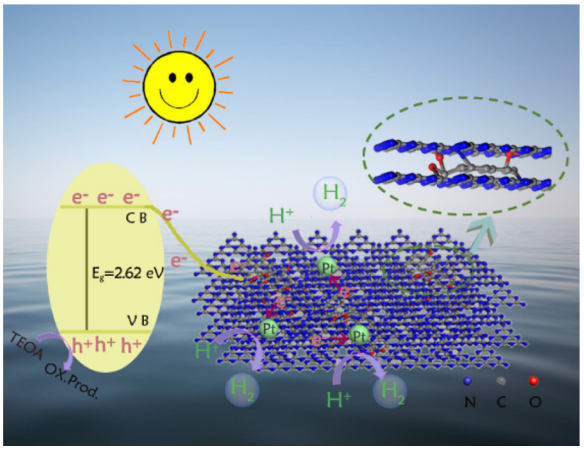

Fig. 10. Schematic illustration of proposed mechanism for the photocatalytic H_2 evolution.

pared with pure g-C_3N_4, the peak of metal-free intercalated g-C_3N_4 are slightly red-shifted, which is consistent with the UV–vis DRS results. Simultaneously, the PL emission intensity decrease sharply, suggesting that the increasing of separation efficiency of charge carriers. This may be attribute to the incorporation of metal-free interlayer into g-C_3N_4, which bridged the interlayer acting as the electron transporter and extended the π-conjugated system of g-C_3N_4. Thus, the migration and separation rate of charge transfer are improved.

Based on the above analyses, a visible-light photocatalytic H_2 evolution mechanism on metal-free intercalated g-C_3N_4 is provided in Fig. 10. Under the visible light illumination, the photo-excitation of electrons and holes are firstly produced in metal-free intercalated g-C_3N_4. The electrons transfer from the valence band to the conduction band, leaving holes in the valence band [27]. With the incorporation of metal-free interlayer into g-C_3N_4, the π-conjugated system would be extended and the bridged oxygen-contained graphitized carbon between g-C_3N_4 interlayer act as an electron transporter, which increase the migration and separation efficiency of photo-excitation of electrons and holes. Additionally, compared with pure g-C_3N_4, the electrons in metal-free intercalated g-C_3N_4 have stronger reduction capability due to the upshift of the conduction band potential. As a consequence, the electron in the conduction band quickly transfer to the surface of g-C_3N_4 and couple with Pt particles. Then the hydrogen ions accept the coupled-Pt electron to produce hydrogen. In the meantime, the holes react with TEOA through oxidation reaction.

4. Conclusions

In summary, the nonmetal oxygen-contained graphitized carbon intercalated g-C_3N_4 photocatalyst has been prepared by thermal polymerization strategy used the β-CD and melamine as the original materials. The optimal photocatalyst shows the photocatalytic H_2 evolution rate is 793 μmol h^{-1} g^{-1}, which is 5 times higher than the pure g-C_3N_4. The enhanced photocatalytic activity results from the introducing metal-free interlayer. It can readily tune the band gap of g-C_3N_4 by controlling the different weight ratio of precursors as well as bridge the interlayer and extend the π-conjugated system of this copolymer contributing to the charge-carrier migration and separation, which are proved by the results of photoluminescent spectrum and photoelectrochemical measurement. In addition, the introducing metal-free interlayer also lead to the larger specific surface, which is another reason for improved photocatalytic activity. This present work opens a new avenue for the development of other high performance, cost-effective and metal-free photocatalysts for the practical photocatalytic application.

Acknowledgements

This work was financially supported by projects of Natural Science Foundation of China (21471040, 21271055, and 21501035), and China Postdoctoral Science Foundation funded project (2015M570298). We acknowledge for the support by Fundamental Research Funds for the Central Universities (HIT. IBRSEM. A.201410), Program for Innovation Research of Science in Harbin Institute of Technology (PIRS of HIT B201508)

Appendix A. Supplementary data

Supplementary data associated with this article can be found, in the online version, at http://dx.doi.org/10.1016/j.apcatb.2016.09.075.

References

[1] Z.J. Han, F. Qiu, R. Eisenberg, P.L. Holland, T.D. Krauss, Science 338 (2012) 1321–1324.
[2] X.B. Chen, S.H. Shen, L.J. Guo, S.S. Mao, Chem. Rev. 110 (2010) 6503–6570.
[3] W. X, M., K, T., A, T., K, X., G, C., JM, D., K, A. M, Nat Mater 8 (2009) 76–80.
[4] G.G. Liu, T. Wang, H.B. Zhang, X.G. Meng, D. Hao, K. Chang, P. Li, T. Kako, J.H. Ye, Angew. Chem. Int. Ed. 54 (2015) 13561–13565.
[5] Q. Han, B. Wang, Y. Zhao, C.G. Hu, L.T. Qu, Angew. Chem. Int. Ed. 54 (2015) 11433–11437.
[6] J. Liu, Y. Liu, N.Y. Liu, Y.Z. Han, X. Zhang, H. Huang, Y. Lifshitz, S.T. Lee, J. Zhong, Z.H. Kang, Science 347 (2015) 970–974.
[7] S.W. Cao, J.X. Low, J.G. Yu, M. Jaroniec, Adv. Mater. 27 (2015) 2150–2176.
[8] X. Wang, X. Chen, A. Thomas, X. Fu, M. Antonietti, Adv. Mater. 21 (2009) 1609–1612.
[9] T. Xiong, W. Cen, Y. Zhang, F. Dong, ACS Catal. 6 (2016) 2462–2472.
[10] H. Gao, S. Yan, J. Wang, Y.A. Huang, P. Wang, Z. Li, Z. Zou, Phys. Chem. Chem. Phys. 15 (2013) 18077–18084.
[11] Y.H. Ng, S. Ikeda, M. Matsumura, R. Amal, Energ Environ Sci 5 (2012) 9307–9318.
[12] W. Zhu, J. Zhang, Z. Jiang, W. Wang, X. Liu, RSC Adv. 4 (2014) 17387–17392.
[13] Y.Y. Chu, Z.B. Wang, J. Cao, D.M. Gu, G.P. Yin, Fuel Cells 13 (2013) 380–386.
[14] B.-H. Han, W. Zhou, A. Sayari, J. Am. Chem. Soc. 125 (2003) 3444–3445.
[15] R.P. Rocha, J.P. Sousa, A.M. Silva, M.F. Pereira, J.L. Figueiredo, Appl. Catal. B: Environ. 104 (2011) 330–336.
[16] M. Sampaio, R. Bacsa, A. Benyounes, R. Axet, P. Serp, C. Silva, A. Silva, J. Faria, J. Catal. 331 (2015) 172–180.
[17] E. Raymundo-Piñero, F. Leroux, F. Béguin, Adv. Mater. 18 (2006) 1877–1882.
[18] N.-J. Kang, D.-Y. Wang, J Mater Chem A 1 (2013) 11376–11383.
[19] X. Xue, Q. Gu, G. Pan, J. Liang, G. Huang, G. Sun, S. Ma, X. Yang, Inorg. Chem. 53 (2014) 1521–1529.
[20] F. He, G. Chen, Y. Yu, Y. Zhou, Y. Zheng, S. Hao, Chem. Commun. 51 (2015) 6824–6827.
[21] Y. Zhou, L. Zhang, W. Huang, Q. Kong, X. Fan, M. Wang, J. Shi, Carbon 99 (2016) 111–117.
[22] Z. Zhang, J. Huang, Q. Yuan, B. Dong, Nanoscale 6 (2014) 9250–9256.
[23] Z.F. Huang, J. Song, L. Pan, Z. Wang, X. Zhang, J.J. Zou, W. Mi, X. Zhang, L. Wang, Nano Energy 12 (2015) 646–656.
[24] M. Li, X. Huang, C. Wu, H. Xu, P. Jiang, T. Tanaka, J. Mater. Chem. 22 (2012) 23477–23484.
[25] T.Y. Ma, S. Dai, M. Jaroniec, S.Z. Qiao, Angew. Chem. 53 (2014) 7281–7285.
[26] A. Sanchez-Sanchez, F. Suarez-Garcia, A. Martinez-Alonso, J.M.D. Tascon, Carbon 70 (2014) 119–129.
[27] W.-J. Ong, L.-L. Tan, S.-P. Chai, S.-T. Yong, A.R. Mohamed, Nano Energy 13 (2015) 757–770.
[28] S.C. Yan, Z.S. Li, Z.G. Zou, Langmuir 25 (2009) 10397–10401.
[29] W.Y. Chen, J. Ji, X.Z. Duan, G. Qian, P. Li, X.G. Zhou, D. Chen, W.K. Yuan, Chem. Commun. 50 (2014) 2142–2144.
[30] L. Sun, M. Yang, J. Huang, D. Yu, W. Hong, X. Chen, Adv. Funct. Mater. 26 (2016).
[31] J.S. Lee, K.H. You, C.B. Park, Adv. Mater. 24 (2012) 1084–1088.
[32] Y. Li, H. Zhang, P. Liu, D. Wang, Y. Li, H. Zhao, Small 9 (2013) 3336–3344.
[33] S. Chu, Y. Wang, Y. Guo, J. Feng, C. Wang, W. Luo, X. Fan, Z. Zou, ACS Catal. 3 (2013) 912–919.
[34] G. Liu, G. Zhao, W. Zhou, Y. Liu, H. Pang, H. Zhang, D. Hao, X. Meng, P. Li, T. Kako, Adv. Funct. Mater. (2016) 1–8.
[35] J.H. Li, B.A. Shen, Z.H. Hong, B.Z. Lin, B.F. Gao, Y.L. Chen, Chem. Commun. 48 (2012) 12017–12019.
[36] J. Ding, L. Wang, Q. Liu, Y. Chai, X. Liu, W.-L. Dai, Appl. Catal. B: Environ. 176 (2015) 91–98.